Available online at www.sciencedirect.com
ScienceDirect
Journal of Power Sources 160 (2006) 542–547
JOURNAL OF POWER SOURCES
www.elsevier.com/locate/jpowsour

Shape-controlled synthesis and lithium-storage study of metal-organic frameworks Zn_4O(1,3,5-benzenetribenzoate)$_2$

Xiaoxia Li, Fangyi Cheng, Shuna Zhang, Jun Chen *

Institute of New Energy Material Chemistry, Nankai University, Tianjin 300071, PR China

Received 11 November 2005; received in revised form 25 December 2005; accepted 5 January 2006
Available online 13 February 2006

Abstract

Polycrystalline metal-organic frameworks Zn_4O(1,3,5-benzenetribenzoate)$_2$ (named as MOF-177) with different morphologies have been controlled synthesized through a solvothermal route. MOF-177 electrodes for lithium storage exhibit a relatively high irreversible capacity in the first discharge process and a much lower reversible discharge–charge capacity in the following electrochemical cycles. The performance of MOF-177 is found not impressive for application in reversible lithium storage. A preliminary reaction mechanism on the basis of transmission electron microscopy (TEM) and X-ray photoelectron spectroscopy (XPS) is proposed to understand the chemical behaviors of the electrode.

Keywords: MOF-177; Lithium batteries; Shape-control synthesis

1. Introduction

The design, synthesis, and application of new materials with novel structure are challenging and meaningful subject to chemists and materials scientists. Recently, intensive researches have been focused on constructing a new class of crystalline porous materials that commonly refer to metal-organic frameworks (MOFs), in which metal ions and clusters are linked by organic units [1]. The successfully preparation of MOFs with high surface areas, high stability, adjustable pore size, and organic functionality has led to their application study for molecular sorption [2–5]. Among the family of MOFs, the newly synthesized Zn_4O(1,3,5-benzenetribenzoate)$_2$ (named as MOF-177) was reported to present exceptional level of surface area and to be capable of absorbing inorganic and organic guest molecules such as H_2, N_2, C_{60}, as well as dyes [6]. Presumably, the numerous pores, cavities, and active sites (ZnO_4 tetrahedron) in MOF-177 may accommodate lithium ions as well. However, to the best of our knowledge, up to now no research has been reported on the employment of MOFs in lithium storage and few if any attempt has been made to the utilization of MOFs for batteries. Since the microstructure and morphology of materials have a great influence on their applications [7] and furthermore, since rechargeable lithium-ion batteries are becoming more and more important as power source for a wide variety of applications in daily life [8–10], herein we are interested in the study of shape-controlled synthesis and lithium storage of MOF-177. It is found that MOF-177 with different morphologies can be prepared by simply controlling the reaction conditions. The electrochemical results reveal that MOF-177 is not suitable for application in reversible lithium storage. A preliminary mechanism of the electrode reactions is also proposed and discussed based on TEM and XPS analysis.

2. Experimental

2.1. Synthesis

The starting materials, 4-methylacetophenone ($CH_3C_6H_4COCH_3$), toluene, triflic acid (CF_3SO_3H), HNO_3, *N*,*N*-diethylformamide (DEF, $HCON(CH_2CH_3)_2$), and $Zn(NO_3)_2{\cdot}6H_2O$ were purchased from Aldrich and used without any further purification. The synthesis of MOF-177 follows a three-step reaction route: preparation of 1,3,5-tris(methylphenyl)benzene, preparation of 4,4′,4″-benzene-1,3,5-triyl-tri-benzoic acid (abbreviated to H_3BTB), the final synthesis of MOF-177, as shown in Scheme 1. In the first step, a mixture of 28.25 g

* Corresponding author. Tel.: +86 22 23506808; fax: +86 22 23509118.
E-mail address: chenabc@nankai.edu.cn (J. Chen).

0378-7753/$ – see front matter © 2006 Elsevier B.V. All rights reserved.
doi:10.1016/j.jpowsour.2006.01.015

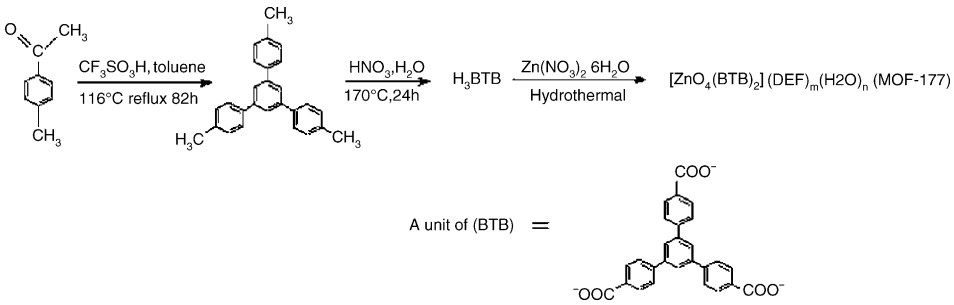

Scheme 1. The depiction of the synthesis process of MOF-177 with three steps.

(0.21 mol) of 4-methylacetophenone and 0.1 mL of triflic acid was dissolved in 140 mL of toluene and then refluxed for 22 h. Then an additional 0.1 mL of triflic acid was added, and the reflux was continued for 60 h. The resultant water was removed through a Dean-Stark trap. The formed concentrated solution was cooled to room temperature to obtain the crude product. Recrystallization from toluene and further re-crystallization from CH_2Cl_2–methanol (2:1) gave 9.88 g of pale yellow needles (41% yield) with the ^{1}H NMR (in $CDCl_3$, ppm): 2.4 (s, 9H), 7.26, 7.29, 7.57, 7.60 (12H), 7.72 (s, 3H). H_3BTB was prepared by combination of the as-synthesized 1,3,5-tris(methylphenyl)benzene (1.0 g, 5.74 mmol), concentrated HNO_3 (1.5 mL), and water (6.0 mL) in a Parr Teflon-lined stainless steel vessel. The reaction mixture was heated to 170 °C for 24 h to give 1.95 g of H_3BTB (77% yield). Polycrystalline MOF-177 were synthesized by a solvothermal reaction of $Zn(NO_3)_2{\cdot}6H_2O$ (0.1214 g, 0.41 mmol) and H_3BTB (0.0307 g, 0.07 mmol) dissolved in DEF (3 mL) in a Parr Teflon-lined stainless steel vessel. The morphology of the final product was controlled by varying the reaction conditions in this step. Four kinds of samples were prepared and named as samples A–D, respectively. For the preparation of samples A and B, the mixture of $Zn(NO_3)_2{\cdot}6H_2O$ and H_3BTB was heated at a rate of 2.0 °C min^{-1} to 100 °C, held at 100 °C for 48 h, and cooled naturally or at a cooling rate of 0.5 °C min^{-1} separately to room temperature to get the product of samples A and B, respectively. Sample C was prepared by heating the mixture to 120 °C at a rate of 2.0 °C min^{-1}, holding at 120 °C for 48 h, and cooling at a speed of 0.1 °C min^{-1} to ambient temperature. While the mixture was heated to 90 °C, kept at 90 °C for 24 h, and cooled down at a rate of 0.1 °C min^{-1}, sample D was obtained. Before further analysis, all the samples were washed with DEF (three times, 2 mL for each time) and dried in air at 120 °C for 2 h.

2.2. Characterization and electrochemical measurement

The as-prepared samples were characterized by powder X-ray diffraction (XRD, Rigaku D/max 2500 X-ray generator, Cu Kα radiation), scanning electron microscopy (SEM, Philips XL-30), transmission electron microscopy (TEM, Philips Tecnai F20, 200 kV), thermogravimetry–differential thermogravimetry (TG–DTG, Model TG 209, Netzsch), and X-ray photoelectron spectroscopy (XPS, Shimadzu, ESCA-3400). Electrochemical tests were carried out using two-electrode cells with lithium metal as the counter electrode. The working electrodes were constructed by compressing the mixture of 85 wt% active materials (samples C and D), 10 wt% acetylene black and 5 wt% polytetrafluoroethylene onto a copper film. The cell assembly was operated in a glove box filled with pure argon. The electrolyte solution consisted of 1 M $LiPF_6$ in a solution of ethylene carbonate (EC), propylene carbonate (PC), and diethyl carbonate (DEC) with the volume ratio of 3:1:1. Discharge–charge measurements were performed at room temperature using a modified Arbin charge–discharge unit. The cells were cycled between 0.05 and 1.6 V at a current density of 50 mA g^{-1}.

3. Results and discussion

3.1. Controlled synthesis

Polycrystalline samples of Zn_4O(1,3,5-benzenetribenzoate)$_2$ are prepared by a solvothermal reaction of $Zn(NO_3)_2{\cdot}6H_2O$ with 4,4′,4″-benzene-1,3,5-triyl-tri-benzoic acid (H_3BTB) in a Teflon-lined stainless steel vessel. The present synthesis strategy is based on literature [6], but in order to evaluate the possibility of shape-controlled synthesis, varied reaction conditions such as temperature, time, concentration of reactants, molar ratio of Zn^{2+} to H_3BTB, as well as the heating and cooling rate are provided. Fig. 1 shows the scanning electron microscope (SEM) images of the as-synthesized four MOF-177 samples. Apparently, the morphologies and dimensions of the product are strongly dependent on the reaction conditions. It is found that the reaction temperature, reaction time and cooling rate play the dominating roles in effecting the final morphology of product. When reacting at 100 °C for 48 h and cooling naturally to room temperature, the product (sample A) is the gathering of numerous microfilaments, as shown in Fig. 1a. A controlled cooling rate of 0.5 °C min^{-1} leads to the formation of MOF-177 cluster (sample B) which is composed of irregular microrods and microneedles (Fig. 1b). Fig. 1c indicates that at an elevated temperature of 120 °C and a slower cooling rate of 0.1 °C min^{-1}, microcuboids (sample C) with regular geometry shape are formed. Meanwhile, Fig. 1d displays a lot of cubic-shaped crystals (sample D) with smooth surface, resulting from lower temperature (90 °C) and shorter reaction time (24 h). The microcuboids are tightly aggregated to each other, and their lengths and widths are not uniform. As a

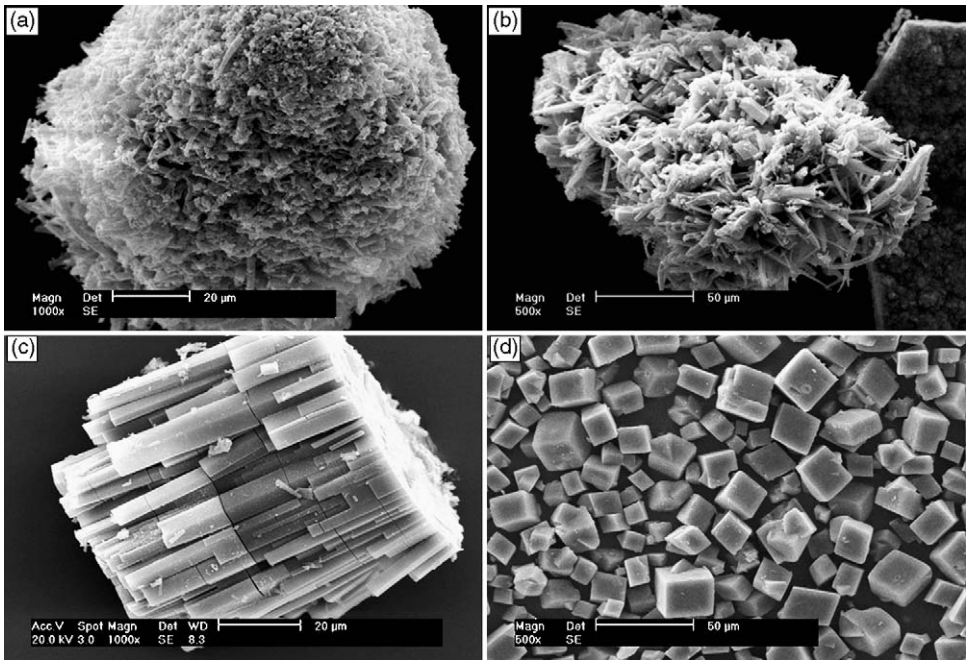

Fig. 1. SEM images of MOF-177 samples result from solvothermal treatment of zinc nitrate and H_3BTB under different reaction conditions. Parts (a–d) correspond to samples A–D, respectively, as outlined in the text.

comparison, the microcubes are dispersive with relatively even dimensions.

Based on the above observations, the shape-controlled synthesis of MOF-177 is achievable by controlling the reaction conditions and in addition, it is preliminarily found that low temperature and short reaction time favor the growth of dispersive crystals and slow cooling rate tends to form geometry regular-shaped product. However, detailed analysis based on more characterization techniques such as in situ morphology study, is needed to further understand the specific crystal growth process in the solvothermal synthesis of MOF-177.

We next emphasize on studying the lithium storage ability of MOF-177. The four samples are characterized by powder XRD, and TG measurement to determine their crystal structure and composition before carrying out the electrochemical tests. As a representative, Fig. 2 shows the XRD and TG–DTG of the obtained microcubes (sample D). XRD pattern of the microcubes in Fig. 2a indicates that the product in our solvothermal synthesis is MOF-177 polycrystal other than single crystal. The intensive peaks appearing at small 2θ angles are characteristics of micro-porous materials which possess numerous tiny pores or cavities. As shown in TG and DTG curves (Fig. 2b), three prominent weight loss steps are observed. The fist two steps of weight loss (31.09%) occur in the range from 50 to 350 °C, which can be attributed to the loss of the guest molecules (H_2O and DEF); the third weight loss of 28.74% appearing between 350 and 500 °C is due to the decomposition of the metal-organic frameworks. These present results are in some what different from that reported by Chae et al. [6]. We deduce that the difference comes from the altered reaction conditions, under which the obtained MOF-177 polycrystals might possess slightly var-

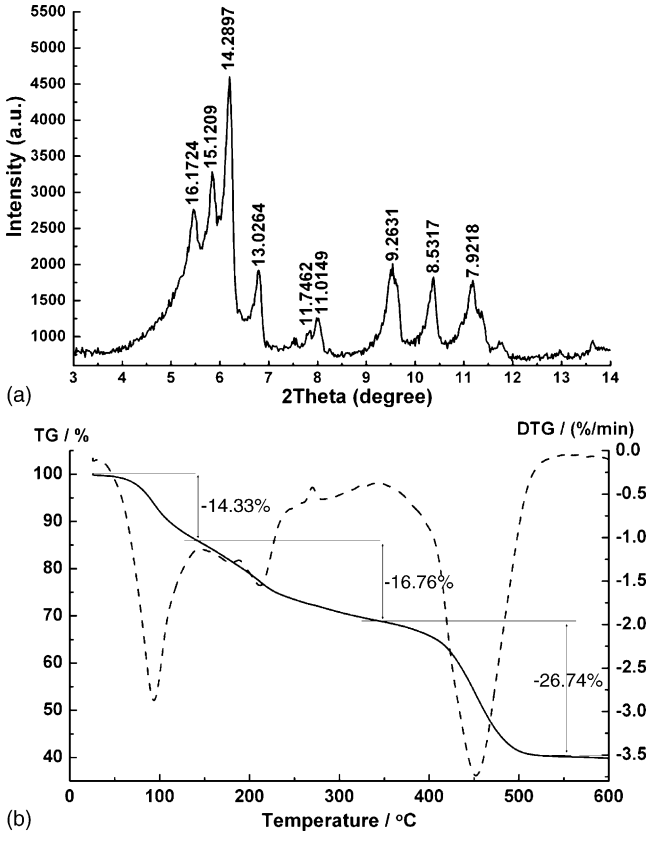

Fig. 2. (a) XRD pattern of the otbained MOF-177 mirocubes prepared through a solvothermal route. (b) TG (solid line) and DTG (dashed line) curves of the microcubes.

ied specific structure or different precise framework periodicity. Furthermore, our pre-treatment of the samples before XRD and TG measurement differs much from that in the above mentioned literature. Based on the TG data, the calculated composition of the as-synthesized product after air dry at 120 °C for 2 h was $Zn_4O(BTB)_2(DEF)_5(H_2O)_1$.

3.2. Lithium storage investigation

A series of metal oxides are found to exhibit excellent electrochemical performances for lithium insertion/deinsertion [11–13], and in particular, some compounds of zinc are reported to deliver high capacity as negative electrode materials in lithium-ion batteries [14–16]. Moreover, MOF-177 has been demonstrated to be capable of hydrogen storage. So we are interested in exploring the possibility of employing MOF-177 as lithium storage materials. The Li/MOF cells made with the as-prepared samples as working electrode and lithium metal as counter electrode are thus assembled and electrochemically investigated.

Fig. 3 shows the discharge/charge curves of two assembled cells composed of the as-synthesized MOF-177 microcubes (sample D) and microcuboids (sample C). Fifty discharge–charge cycles are tested, but for the sake of clarity, the curves of the third to 50th cycles are not shown here since they are almost identical to that of the second cycle. In essence, the discharge and charge curves for the two samples are analogous to each other. The range of potential turning in the discharge curves occurs between 1.6 and 0.1 V while it appears between 0.3 and 1.3 V in the charge curves. Such low potential range is suitable for the application of MOF-177 as negative active materials in lithium-ion batteries. The discharge curves of the microcubes and microcuboids present almost the identical shape. However, the former possesses a slightly higher charge plateau than that of the latter. In addition, the microcubes deliver relatively higher charge and discharge capacities. We speculate these differences

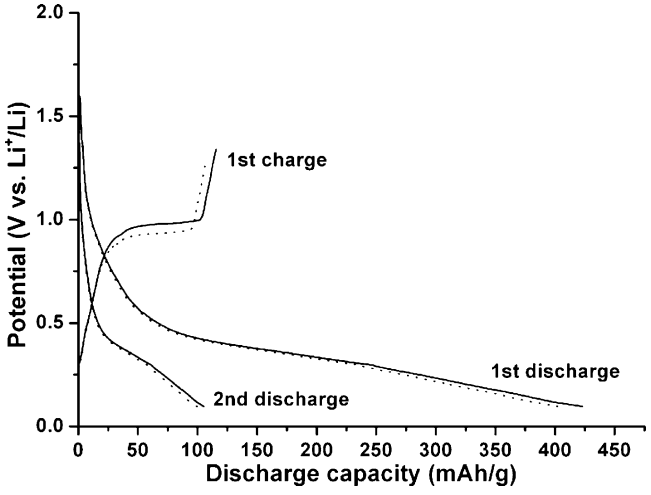

Fig. 3. Discharge–charge performances of the electrodes made with the as-synthesized MOF-177 microcubes (solid lines) and microcuboids (dotted lines). The discharge/charge process was carried out under constant current density of 50 mA g^{-1} at 20 °C.

are due to the different shapes and sizes of the two kinds of obtained samples. As seen in the SEM images (Fig. 1), the as-prepared MOF-177 microcubes are dispersive, whereas the microcuboids are aggregated to each other. The dispersive form favors the contact between the active material and electrolyte, hence the utilization efficiency of microcubes is higher than that of microcuboids to some extent, resulting in a slightly higher capacity in the electrode process.

It should be noted that the capacity of MOF-177 in the second discharge process is only 105 mAh g^{-1} while it is more than 400 mAh g^{-1} in the first cycle. Compared with the capacity of the first and second cycles, the capacity deterioration reaches as high as three fourths. Thus, in the initial discharge, an irreversible electrochemical process which causes the great capacity fade takes place. After a preliminary test of 50 consecutive cycles at 100% depth of discharge and charge, the capacities of the electrodes for the microcubes and microcuboids decreased by 2% and 2.5%, respectively, referred to that of the second cycle, showing the cycling stability after the first irreversible discharge process. The important point is how to explain the above electrochemical behaviors of the MOF-177 electrode. It is obvious that the irreversible or reversible Li intercalation/deintercalation is much different from the previously reported sorption/desorption of neutral molecules occurring in MOFs, because the Li insertion/desertion process involves not only physical change but also electrochemical reduction/oxidation. The tentative related interpretations are proposed as follows.

At first, we think that the high capacity of the first discharge process derives mainly from the large amount of cavities in MOF-177 and from the contained guest molecules such as DEF and H_2O. Two kinds of lithium are envisaged to exist in MOF-177 electrode. One is Li^+ that comes from the electrolyte. The other is Li which results from the reduction of inserted Li^+, as will be discussed later. Both kinds of lithium can enter and reside in the numerous micropores during the discharge/charge process. The intercalated Li^+ or resultant Li then react with DEF and H_2O which contain active protons, giving out electrons or receiving electrons from anode (refer to metal counter electrode) through outer circuit. Since such reactions are irreversible, high capacity is observed only in the first cycle. On the other hand, if the MOF-177 samples have not been air dried before assembling them into cell, much larger capacity will be obtained due to greatly higher content of guest molecules. The reported composition of MOF-177 is $Zn_4O(BTB)_2(DEF)_{15}(H_2O)_3$, in which the content of guest molecules is much higher than that calculated from our analysis. Therefore, given that the guest molecules are preserved in the frameworks, higher capacity is expected. As we know, many chemical reactions involve oxidation/reduction process, but merely when the redox reactions take place in electrode system can the electric power be utilized in control. The metal-organic frameworks with active component which will consume electrons are capable of providing reactive sites for electrode process. From this point of view, although the high capacity of MOF-177 is limited in irreversibility, it is of interest to exploit the energy-storage possibility of such kinds of porous metal-organic compounds, especially those with low molecular weight.

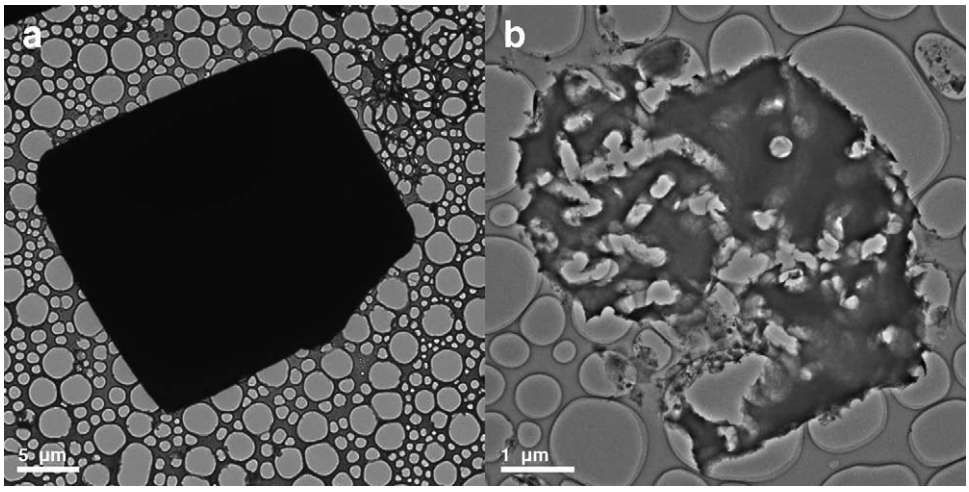

Fig. 4. Typical TEM images of the MOF-177 sample measured before electrochemical tests (a) and examined after the first discharge process (b).

3.3. Mechanism discussion

Another interesting point is the cycling ability of MOF-177 electrode after the first discharge process. A reversible capacity of about 105 mAh g^{-1} is gained and the corresponding discharge potential plateau is 0.35–0.1 V in the second cycle and thereafter. Based on the capacity and potential values obtained in Fig. 3, we speculate that the involved reactions in the MOF-177 electrode could be expressed as:

$$Zn_4O(BTB)_2\cdot(DEF)_m(H_2O)_n + e + Li^+ \rightarrow Zn + Li_2O \quad (1)$$

$$DEF + H_2O + e + Li^+ \rightarrow Li_2(DEF) + LiOH \quad (2)$$

$$Zn + Li^+ + e \leftrightarrow LiZn \quad (3)$$

The reaction described in Eq. (1) is destructive to the frameworks of MOF-177. TEM observations (Fig. 4) taken before and after electrochemical tests confirm the break down of the structure. As seen in Fig. 4a and b, after the electrode process, the original cubic-like solid no longer preserves its integrity. The decomposition of MOF-177 also proves that the capacity loss is partly due to the electrochemical reactions which cause irreversible structural changes. Reaction (2) is one of the reasons that lead to the high discharge capacity in the first cycle. Reaction (3) is believed to be reversible and be responsible for the remained capacity around the level of 100 mAh g^{-1}. The formation of Li is surprising because the reaction seems thermodynamically infeasible. However, it should be noted that after reaction (1), the destruction of MOF-177 frameworks leads to the formation of nanosized zinc particles, and nanosized materials usually exhibit extremely high activities [12]. The zinc nanoparticles are thus believed to enhance the electrochemical activity towards the formation of Li–Zn nanoalloy.

The formation of zinc and Li–Zn alloy has been reported to occur in different electrochemical systems [14,17]. In the present study, we also found the formation of zinc, which is directly confirmed by XPS analysis, as shown in Fig. 5. The XPS in Fig. 5a and b presents Zn 2p spectra for the MOF-177 samples performed before and after the first electrochemical discharge, respectively. It can be seen that XPS spectra before and after the lithium storage are slightly different, indicating the varied chemical state of zinc element. In Fig. 5a, the two peaks appearing at 1044.7 and 1021.7 eV can be assigned to Zn $2p_{1/2}$ and $2p_{3/2}$, respectively [18]. Both the location of the two lines coincides well with that of ZnO, revealing the ionic state of Zn in MOF-177 samples before lithium take-up. As a comparison, for the sample after the first discharge, the binding energies of Zn $2p_{1/2}$ and $2p_{3/2}$ shift towards a lower energy of 1044.6 and 1021.5 eV, respectively. In addition, the separation of the binding energy between $2p_{1/2}$ and $2p_{3/2}$ increases from 23.0 to 23.1 eV. These two characteristics imply the formation of metallic zinc [18] during the electrochemical reactions. Therefore, Li–Zn nanoalloy forms in the discharge process, while the de-alloying reaction takes place in the charge process. The two steps are reversible, giving a charge/discharge capacity of about 100 mAh g^{-1}, a discharge voltage range of 0.35–0.1 V, and a charge plateau of 0.8–1.0 V. As a result, the above expressed Eq. (3) explains the cycling ability of MOF-177 electrode after the first discharge process. Further studies are still underway to learn

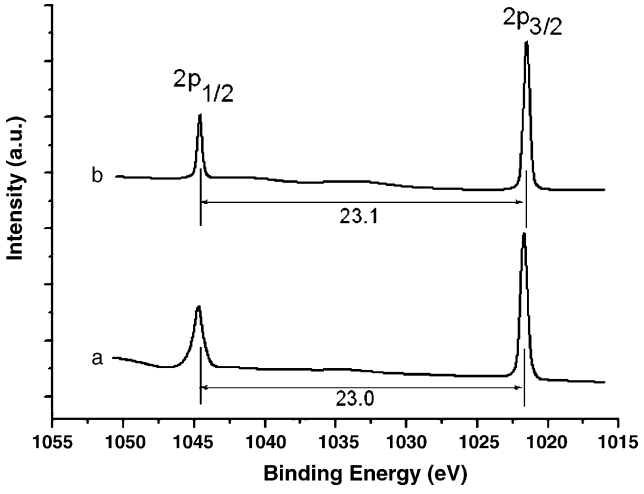

Fig. 5. Zn 2p XPS spectra of the MOF-177 samples taken before (a) and after (b) electrochemical discharge process from the assembled electrodes.

more about the electrochemical behavior of such metal-organic materials.

4. Conclusions

Shape-controlled synthesis of metal-organic frameworks Zn_4O(1,3,5-benzenetribenzoate)$_2$ (namely MOF-177) was reported by a facile solvothermal route. Furthermore, it has been found in the electrochemical tests that the obtained MOF-177 samples exhibit an irreversible high capacity in the first discharge process and show good cycling ability after the first cycle but the capacity is relatively low. TEM analysis indicates the structure destruction of the sample after lithium storage and XPS spectra prove the formation of metallic zinc in the discharge process. Therefore, the performance of MOF-177 applied in reversible lithium storage was not impressive since the cycling capacity is limited. The present results should shed a preliminary light upon the lithium-storage study of porous metal-organic materials. Moreover, the possibility of employing MOFs with low molecular weight in the storage of other light metal such as Na, Mg, or Al is of great interest and worth consideration.

Acknowledgments

This work was supported by the Outstanding Young Scientific Foundation of NSFC (20325102) and National Key Basic Research Program (2005CB623607).

References

[1] M. Eddaoudi, D.B. Molor, B. Li, B.L. Chen, T.M. Reineke, M. O'Keeffe, O.M. Yaghi, Acc. Chem. Res. 34 (2001) 319.
[2] M. Konda, T. Okubo, A. Asami, S. Noro, T. Yoshitomi, S. Kitagawa, T. Ishii, H. Matsuzaka, K. Seki, Angew. Chem. Int. Ed. 38 (1999) 140.
[3] X.B. Zhao, B. Xiao, A.J. Fletcher, K.M. Thomas, D. Bradshaw, M.J. Rosseinsky, Science 306 (2004) 1012.
[4] L. Pan, M.B. Sander, X.Y. Huang, J. Li, M. Smith, E. Bittner, B. Bockrath, J.K. Johnson, J. Am. Chem. Soc. 126 (2004) 1308.
[5] B. Panella, M. Hirscher, Adv. Mater. 17 (2005) 538.
[6] H.K. Chae, D.Y. Siberio-Pérez, J. Kim, Y. Go, M. Eddaoudi, A.J. Matzger, M. O'Keeffe, O.M. Yaghi, Nature 427 (2004) 523.
[7] F.Y. Cheng, J. Chen, P.W. Shen, J. Power Sources 150 (2005) 255.
[8] D. Guyomard, J.M. Tarascon, Adv. Mater. 6 (1994) 408.
[9] M.S. Whittingham, Chem. Rev. 104 (2004) 4271.
[10] H. Tsutsumi, H. Higashiyama, K. Onimura, T. Oishi, J. Power Sources 146 (2005) 345.
[11] B.B. Owens, S. Passerini, W.H. Smyrl, Electrochim. Acta 45 (1999) 215.
[12] P. Poizot, S. Laruelle, S. Grugeon, L. Dupont, J.M. Tarascon, Nature 407 (2000) 496.
[13] G.X. Wang, Y. Chen, L. Yang, J. Yao, S. Needham, H.K. Liu, J.H. Ahn, J. Power Sources 146 (2005) 487.
[14] X.B. Zhao, G.S. Cao, Electrochim. Acta 46 (2001) 891.
[15] J.L. Tirado, Mater. Sci. Eng. R 40 (2003) 103.
[16] H. Li, X.J. Huang, L.Q. Chen, Solid State Ionics 123 (1999) 189.
[17] Z.W. Fu, Y. Wang, X.L. Yue, S.L. Zhao, Q.Z. Qin, J. Phys. Chem. B 108 (2004) 2236.
[18] C.D. Wagner, W.M. Riggs, L.E. Davis, J.F. Moulder, G.E. Muilenberg, Handbook of X-Ray Photoelectron Spectroscopy, Perkin-Elmer Corp., Minnesota, 1978.